JMEPEG
https://doi.org/10.1007/s11665-024-09424-4

1059-9495/$19.00

ORIGINAL RESEARCH ARTICLE

Investigation of the Combined Effects of Stress Concentrations and Plasma Nitriding Parameters on the Fatigue Performance of AISI 4140 Low Alloy Steel

F. Yılan and H. Kovacı

Submitted: 15 September 2023 / Revised: 10 January 2024 / Accepted: 18 February 2024

The fatigue performance of machine parts under cyclic loads is significantly reduced by notches, cracks and geometric irregularities on their surfaces. Therefore, it is necessary to eliminate the notch effect, which is effective on the formation of fatigue cracks. In this study, it is aimed to enhance the fatigue strength of notched parts via plasma nitriding. Four various radii (r = 1, 2, 4 and 8 mm) variations were created from AISI 4140 steel with theoretical stress concentration factors (K_t) of 1.63, 1.41, 1.27 and 1.19, respectively. Then, the samples were plasma nitrided at 480 °C for 2 h and 9 h. The morphological, structural and mechanical properties of the samples were characterized by SEM, XRD and microhardness tester. The fatigue tests were performed using a rotating bending fatigue test device. All plasma nitrided parts exhibited higher fatigue strength compared to untreated samples and the level of this increase decreased with increasing K_t. The fatigue properties of plasma nitrided parts improved in comparison to untreated parts, depending on the residual stresses, microhardness and diffusion layer thickness. Consequently, it was found that the fatigue limit improvement up to 72% was achieved in the samples with the lowest K_t and nitrided for long periods.

Keywords fatigue, notch effect, plasma nitriding, stress concentration

1. Introduction

Machine parts operating under cyclic loads are at serious risk of fatigue and it is well-known that fatigue causes the premature failure of materials. Surface properties and geometric properties of materials are among the most important factors affecting fatigue. Fatigue cracks in machine elements usually initiate from the surface irregularities which have high stress concentrations. Therefore, the calculation of theoretical stress concentrations is important (Ref 1, 2). In particular, geometric irregularities called notches are at the forefront of these factors. Stress concentrations occur in the regions of these geometric irregularities and fatigue damage frequently starts from the root of the notches (Ref 3-5). The fatigue limit of the notched parts decreases with the increase of stress concentration (K_t) values and the notch affects the crack formation and propagation life of materials. In addition, the variation of crack propagation life depends on the stress concentration factor, which is the measure of notch effect (Ref 6-9). If the notch effect is inevitable due to geometrical constraints, the fatigue properties of materials should be improved by utilizing beneficial residual stresses, decreasing the stress intensities, increasing the hardness of these regions and reducing the grain size (Ref 10-12).

Fatigue damage usually starts at or near the surface of materials and therefore, some thermochemical and mechanical surface treatments are performed to enhance the fatigue, wear, and corrosion properties of machine elements (Ref 13-18). In order to improve the fatigue strength of materials, plasma nitriding (PN), which is a well-known thermochemical surface treatment, is used frequently. Many different studies were performed to examine the effect of the plasma nitriding on the fatigue strength of materials (Ref 19-22). These studies commonly pointed out that the fatigue strength of materials is improved by plasma nitriding due to high compressive residual stresses, hard surface and inner surface layers and hard nitride phases. Also, some studies focused on the investigation of the effects of plasma-based surface treatment on the notch fatigue strength of materials. Akita and Tokaji (Ref 3) investigated the fatigue limit of the carburized notched samples with different K_t values. The study showed that the formation of cracks was prevented by limiting the shear deformation on the notch root and the fatigue strength of the material was improved by carburizing. Peng et al. (Ref 23) reported the influences of low temperature carburization on the fatigue strength of notched 316L samples with two different K_t values. After the carburizing, the carbon atoms were evenly distributed on the material surface and did not affect the notch shape. Low temperature carburizing significantly improved the notch fatigue strength. In a different study, the notch fatigue strength of plasma nitrided, tempered and quenched (Q&T) samples made of steel were examined in seawater. When the S-N curves were examined, it was observed that seawater suppressed the fatigue limit and

F. Yılan, Department of Mechanical Engineering, Faculty of Engineering and Architecture, Kırşehir Ahi Evran University, Kırşehir, Turkey; and **H. Kovacı**, Department of Mechanical Engineering, Faculty of Engineering, Ataturk University, Erzurum, Turkey. Contact e-mail: halim.kovaci@atauni.edu.tr.

Published online: 15 April 2024

Graphical Abstract

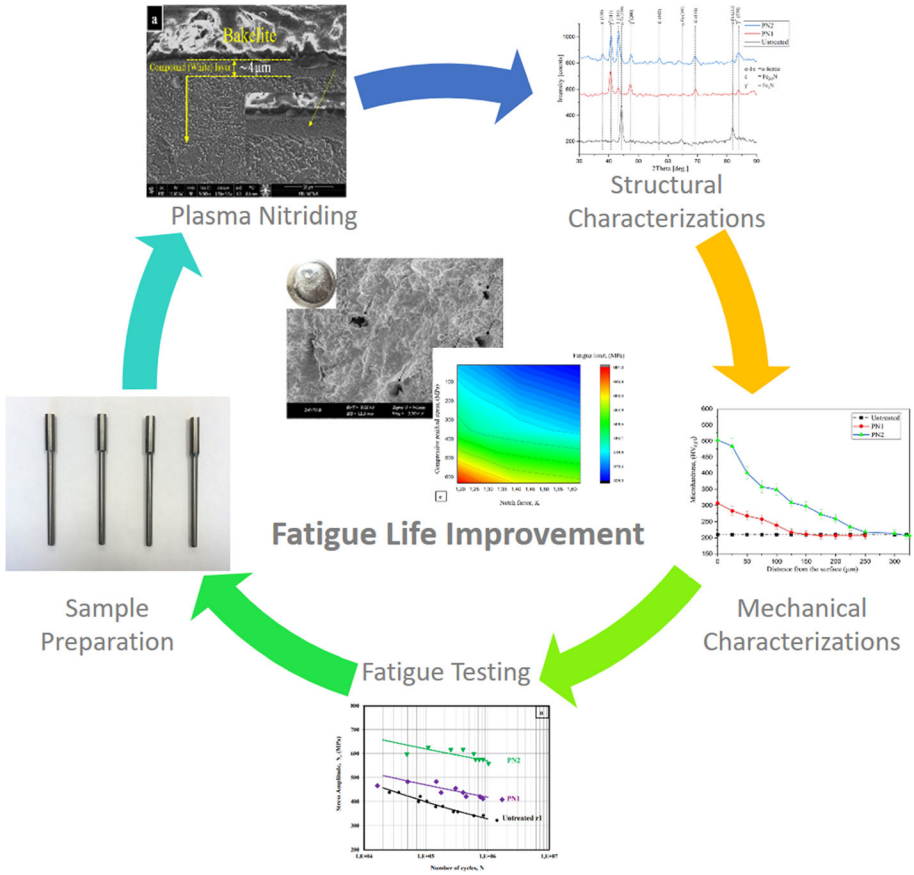

decreased the fatigue limit of the notched PN and Q&T samples (Ref 24). In another study, the influences of plasma nitriding on the notch effect and fatigue limit of SACM 645 steel were investigated. The fatigue properties were improved by nitriding because fatigue crack started under the nitride layer with the effect of compressive residual stresses on the surface and the crack initiation was delayed. The increase in K_t due to the notch effects decreased the fatigue strength (Ref 25). Shengwei et al. Ref 26 reported that they correlated fatigue performances with different carburizing heat treatments on 18CrNiMo7-6 steel. Notched specimens exhibited a significant improvement in fatigue strength up to 128% by carburizing (K_t = 3.46).

As mentioned so far, there are inevitably many geometric changes in machine elements, namely irregularities that can cause notch effect and fatigue originates due to stress concentrations caused by these irregularities. Therefore, surface modification methods are expected to be effective to eliminate the notch effect. Also, as it can be seen in earlier literature studies, many studies were performed to understand the influences of plasma nitriding on the fatigue properties of materials. Also, some preliminary studies were carried out to show that plasma nitriding improved the notch fatigue strength of the materials but these studies were performed generally by considering only one or two plasma nitriding and notch parameters. However, the combined effects of plasma nitriding and stress concentration/notch effects on the fatigue properties of materials have not been investigated by considering different notch and plasma nitriding parameters in detail yet. From this point of view, it is aimed to examine the combined effects of stress concentrations and plasma nitriding on the fatigue properties of AISI 4140 low alloy steel in this study. A detailed analysis was performed to determine the combined and multiple effects of plasma nitriding and notches on fatigue limit of the materials. For this purpose, four different notch variations (r = 1, r = 2, r = 4 and r = 8 mm) were created in AISI 4140 low alloy steel samples, which is used in different industries and many engineering applications like gears, automotive crankshafts, landing gear parts, etc., with theoretical stress concentration factors (K_t) of 1.63, 1.41, 1.27 and 1.19, respectively. Then, the samples were plasma nitrided at 480 °C for 2 h and 9 h in a gas mixture of 25% N_2-75% H_2. SEM and XRD were used for the characterization of the notched parts. Besides, mechanical properties of the samples were determined via rotating bending fatigue test device and microhardness tester.

2. Experimental Details

AISI 4140 low alloy steel was used as a substrate in this study. Tables 1 and 2 show the chemical composition and mechanical properties of this material, respectively. The samples were designed in four various radius (1, 2, 4, 8 mm) with K_t values of 1.63, 1.41, 1.27 and 1.19 respectively Ref 4, 9, 27-29, to promote cracking from the entire circumference to the center to create a circular pattern. All samples were produced on CNC lathes according to DIN 50113 standard (Ref 30) and the specimen geometries are shown in Fig. 1. The prepared notch samples were normalized at 850 °C for 30 h

and their surfaces were polished. Before plasma nitriding, surfaces of all the specimens were cleaned in acetone. The specimens were subjected to plasma nitriding for 2 h and 9 min at 480 °C in a gas mixture of 25% N_2 and 75% H_2 under 5 × 10^2 Pa constant pressure in the I-Nit industrial plasma nitriding furnace (İstanbul Isıl İşlem Ltd. Şti.). PN1 and PN2 denote the plasma nitrided samples at 480 °C for 2 h and 9 h, respectively.

The phase analyses were carried out using an x-Ray diffractometer at 40 kV and 40 mA with a wavelength λ=1.54 Å with Co- K α radiation. The scan angle (2 θ) was chosen between 30 ° and 90 °. In addition, the residual stress values were determined with the $\sin^2 \omega$ method. Three measurements were performed at $\omega = 5°$, $\omega = 10°$ and $\omega = 15°$ for each sample groups. When measuring residual stress, since the wavelength and diffraction angles of the x-ray source used in the XRD device are known, (d) spacing can be determined using Bragg's law. When the $\sin^2 \omega$ graph was drawn against the distance (d), it was stated that the slope of the curve was proportional to the stress. Residual stress measurements were carried out based on this principle. Phase analyses and residual stress measurements were performed using the GNR-Explorer XRD system. Some of the samples prepared for fatigue tests were cut to 8 mm in diameter and 10 mm in length to be used in structural and morphological examinations. Since the samples are in sizes that cannot be easily held by hand, the mounting process has been considered necessary. In this context, the samples were grinded with 240, 320, 600, 800, 1000 and 1200 grinding papers, respectively. They were polished with 3 μm alumina powder and then etched with 3% Nital at room temperature for 10 s. SEM (Zeiss Sigma 300 and FEI Quanta-FEG 50) devices were used to investigate cross-sections and fatigue fracture surfaces of samples. Surface hardness values were determined by using a Shimadzu HMV-G microhardness tester at a dwell time of 10 s and a constant load of 50 g, according to ASTM E384-11 (Ref 31). The hardness of each specimen was measured at least five times before and after plasma nitriding. The hardness measurements were performed from surface to core in plasma nitrided samples. Surface roughness of the samples was measured using Kla Tencor Stylus Profiler P7. Five measurements were taken on each sample and their average values were given.

Effects of plasma nitriding on fatigue properties of materials were investigated in this study by means of stress life approach. Stress life approach investigates all fatigue life of a component from the beginning of fatigue to final fracture. In the stress life approach, as well known, fatigue life of a material is defined by S-N (stress-number of cycles) curves. Untreated and plasma nitrided notched samples were subjected to fatigue by a rotating bending fatigue test machine under constant stress amplitude loading. Rotating bending limits were determined under laboratory air conditions (~ 21 °C and 50% ambient humidity air) operating a sinusoidal frequency of 50 Hz (3000 rpm) and a stress ratio of $R = -1$. The fatigue tests were terminated at each applied stress level up to failure or up to about 10^6 cycles, as performed in preceding studies (Ref 32-34). In order to assess the stress amplitude of each group of samples, 10-12 specimens were used and at least two specimens were tested at each stress level. ASTM E739-91(2004)e1 standard (Ref 35) procedure was carried out to represent the results of statistical analysis and to confirm the fatigue limit with 95% confidence level/band for Wöhler's curve, as in preceding studies (Ref 19, 36). S-N equation for all fatigue test conditions and fatigue limit value for 10^6 cycles are tabulated in Table 3.

Table 1 The chemical composition of AISI 4140 steel used in this study, wt.%

C	Mo	Mn	P	S	Cr	Si	Fe
0.41	0.20	0.75	0.025	0.02	0.95	0.22	Balance

Table 2 Mechanical properties of AISI 4140 steel

Ultimate stress, MPa	Yield stress, MPa	Elastic modulus, GPa	Hardness, HV
650	420	205	210

3. Results and Discussions

3.1 Structural Characterization

XRD graphs of untreated and plasma nitrided samples are given in Fig. 2. The XRD results show that the untreated

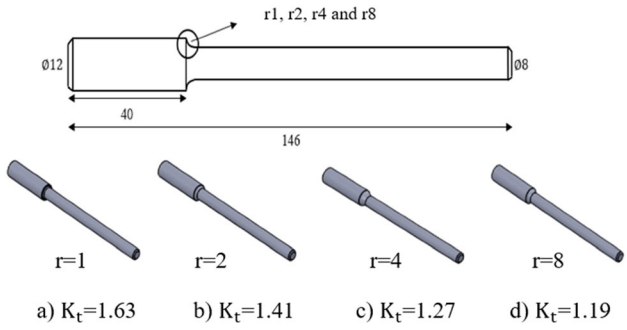

(a)

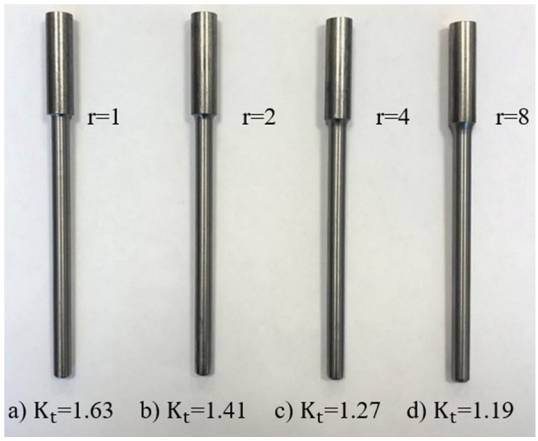

(b)

Fig. 1 The detailed specimen geometry used in rotating bending fatigue tests: (a) notch geometries and (b) manufactured specimens

Table 3 The S-N equations, 95% confidence interval of fatigue limit and the fatigue limit values for all fatigue test conditions for 10^6 cycles

Specimens	Equation of S-N curve	95% Confidence interval	Fatigue limit at 10^6 cycles, MPa	*Change in fatigue limit, %
Untreated-r1	$\mathrm{Log}N = 35,80307 - (11,84303 \times \mathrm{log}S)$	313-335	328	…
Untreated-r2	$\mathrm{Log}N = 32,32581 - (10,33870 \times \mathrm{log}S)$	330-360	352	…
Untreated-r4	$LogN = 37,98709 - (12,36773 \times \mathrm{log}S)$	375-392	386	…
Untreated-r8	$\mathrm{Log}N = 33,28002 - (10,48113 \times \mathrm{log}S)$	390-411	401	…
PN1-r1	$\mathrm{Log}N = 51,54983 - (17,45535 \times \mathrm{log}S)$	395-410	407	+ 24
PN1-r2	$LogN = 50,56394 - (16,91223 \times \mathrm{log}S)$	425-440	432	+ 22
PN1-r4	$\mathrm{Log}N = 60,14502 - (20,38749 \times \mathrm{log}S)$	448-465	482	+ 17
PN1-r8	$\mathrm{Log}N = 55,69554 - (18,52029 \times \mathrm{log}S)$	460-476	465	+ 15
PN2-r1	$\mathrm{Log}N = 87,57343 - (29,62786 \times \mathrm{log}S)$	559-572	567	+ 72
PN2-r2	$\mathrm{Log}N = 85,18704 - (28,55403 \times \mathrm{log}S)$	585-602	593	+ 69
PN2-r4	$LogN = 109,99476 - (36,98385 \times \mathrm{log}S)$	640-656	650	+ 68
PN2-r8	$\mathrm{Log}N = 101,82518 - (33,73211 \times \mathrm{log}S)$	668-698	691	+ 72

*"The values of % change in fatigue limit" is calculated with reference to the fatigue life of each notch geometry in the untreated state.

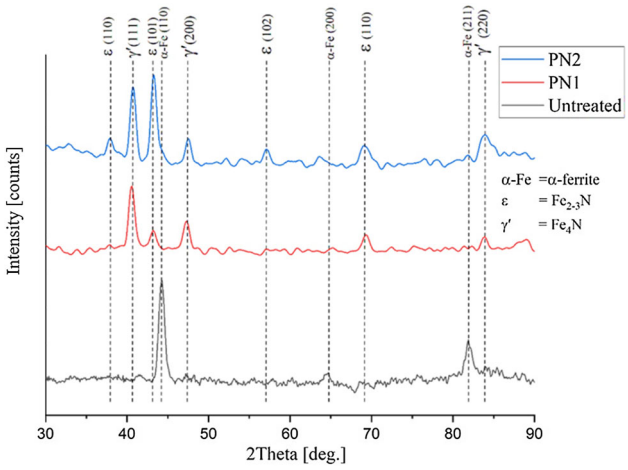

Fig. 2 XRD patterns of untreated and plasma nitrided AISI 4140 steel at different treatment time for 480 °C

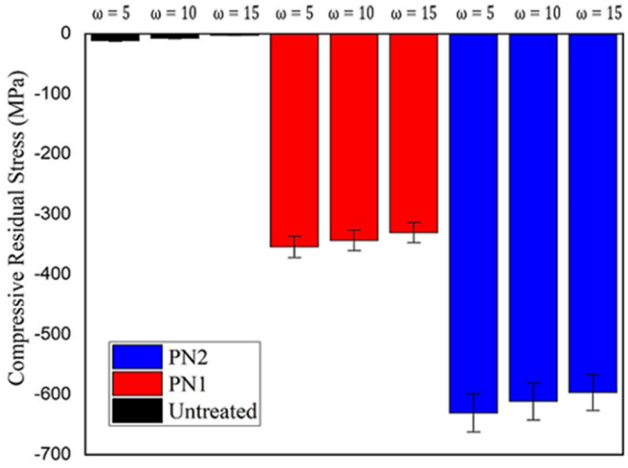

Fig. 3 Residual stresses measured from plasma nitrided specimens at different incident angles

specimen has only α-ferrite peaks. After the plasma nitriding process, it was observed that the α-ferrite peaks disappeared. At the same time, multi-phase high density ε- Fe_{2-3} N (HCP) and $\gamma\prime - Fe_4$ N (FCC) were observed in the nitrided samples (Ref 36-38). The process time essential for the diffusion of the formed phases in plasma nitriding. The diffusion of nitrogen atoms increased with increasing process time, so the formation of iron nitride phases in the material became easier. Therefore, it was determined that the intensities of the peaks of both ε- Fe_{2-3} N and $\gamma\prime - Fe_4$ N phases increased with the increasing treatment time at 480 °C.

The residual stresses values measured from untreated and plasma nitrided specimens are shown in Fig. 3 and tabulated in Table 4. Residual stresses can be tensile or compressive in the structure depending on the direction of the force. Tensile residual stresses are undesirable in fatigue because it facilitates the formation of fatigue damage. Compressive residual stresses increase the fatigue strength of materials by delaying the initiation of fatigue cracks. Therefore, tensile stresses are detrimental for fatigue, while compressive stresses are beneficial (Ref 39). Plasma nitriding changes stress state and creates residual stresses in modified layers. Compressive residual stresses form in AISI 4140 steel samples, with high values obtained at longer times. Residual stresses reduce from surface to core due to decreasing diffusion rate. Three glancing angles were used to measure residual stress changes, with lower values obtained at higher angles due to deeper x-Ray beams. The residual surface stress of the untreated specimen is, on average, − 12 MPa. After plasma nitriding, the amount of compressive residual stresses increased and the maximum surface residual stress was determined in the PN2 sample. In this context, the residual stresses increase due to increasing plasma nitriding time. However, the value of residual stresses measured with increasing angle of incidence decreased for all conditions. This is due to the decrease of N diffusion from the surface to the core of the material. The low-incidence angles of x-rays only count

Table 4 Layer thickness, microhardness and residual stress values of untreated and plasma nitrided samples

Specimens	Plasma nitriding			Thickness, μm		Hardness	Average residual stress, MPa		
	Temp., °C	t, h	Gas mixture, %	Compound	Diffusion	$HV_{0,05}$	ω=5°	ω=10°	ω=15°
PN1	480	2	25%N_2 + 75%H_2	2-4	140-170	300-320	− 355	− 344	− 331
PN2	480	9	25%N_2 + 75%H_2	4-7	290-330	490-530	− 631	− 612	− 597
Untreated	…	…	…	…	…	200-220	− 12	− 8	− 3

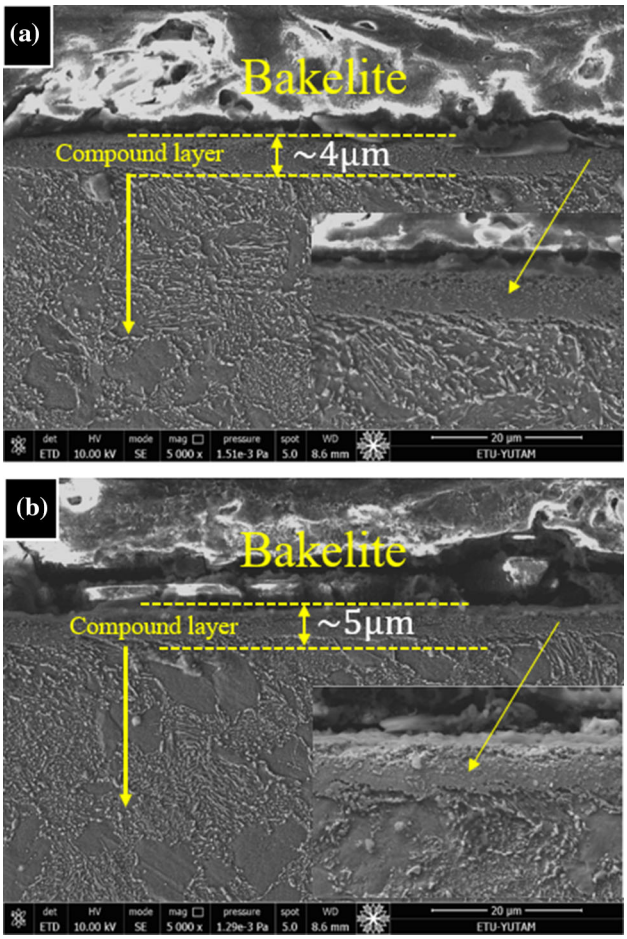

Fig. 4 The cross-section SEM images of plasma nitrided specimens: (a) 480 °C for 2 h-PN1 and (b) 480 °C for 9 h-PN2

the residual stress formed on the surface. For this reason, it cannot reach deeper distances.

Cross-section SEM images of plasma nitrided specimens are shown in Fig. 4. The compound layer in the structure formed after the plasma nitriding is visually distinguished from the substrate with a clear line in a homogeneous thickness. When plasma nitriding is performed at 480 °C for 2 hours, the nitride layer thickness is 4 μm on average. The average value of the thickness increases to 5 μm, for 9 hours. The diffusion coefficient of N in steels is low at a low process time. According to these results, it could be said that the increase in plasma nitriding time did not affect the compound layer thickness considerably.

The relationship between microhardness and distance from the surface of untreated and plasma nitrided are given in Fig. 5. Plasma nitriding resulted in a significant improvement in both

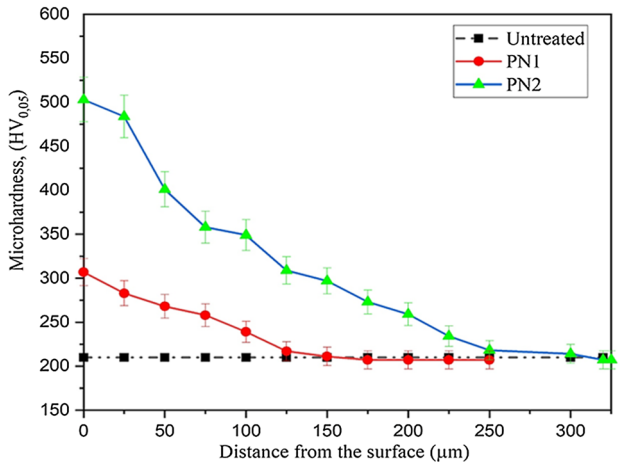

Fig. 5 Microhardness values vs. distance graph of plasma nitrided specimens

the hardness and diffusion zone thickness of the AISI 4140 steel. While the surface hardness value of untreated samples was determined as 210 $HV_{0,05}$ on average, the surface hardness of PN1 and PN2 was 307 $HV_{0,05}$ and 503 $HV_{0,05}$ on average, respectively. Accordingly, approximately 50% and 140% hardness increase was obtained in comparison to the untreated sample. In plasma nitrided samples, the microhardness values decrease from the surface inwards as the dissolved nitrogen concentration in ferrite and metal nitrides decreases. The thickness of diffusion zones are approximately 150 μm for PN1 and 320 μm for PN2 (Fig. 6). The thickness of the diffusion zone increases because the N atoms will have adequate time to diffuse into the steel with longer treatment times (Ref 40). As a result, it can be inferred that the surface hardness of AISI 4140 is improved by plasma nitriding. In addition to these analyses, the surface roughness values of samples were measured. Average roughness value (Ra) of untreated samples were measured as 0.12 μm, whereas 0.17 and 0.22 μm values for obtained for PN1 and PN2, respectively. As it was expected, surface roughness values of the samples increased with plasma nitriding and the increasing process time provided further increment.

3.2 Fatigue and Fractography Results

S-N (Wöhler) curves of untreated notched samples according to the ASTM E739-91(2004)e1 standard Ref 35 are given Fig. 7. According to the graph, an increase in fatigue life was observed due to the increase in the notch radius value. Fatigue limit of untreated r8 (r = 8 mm and K_t = 1.19) notched sample is higher than the fatigue limits of untreated r4 (r = 4 mm and K_t = 1.27), r2 (r = 2 mm and K_t = 1.41) and r1 (r = 1 mm and

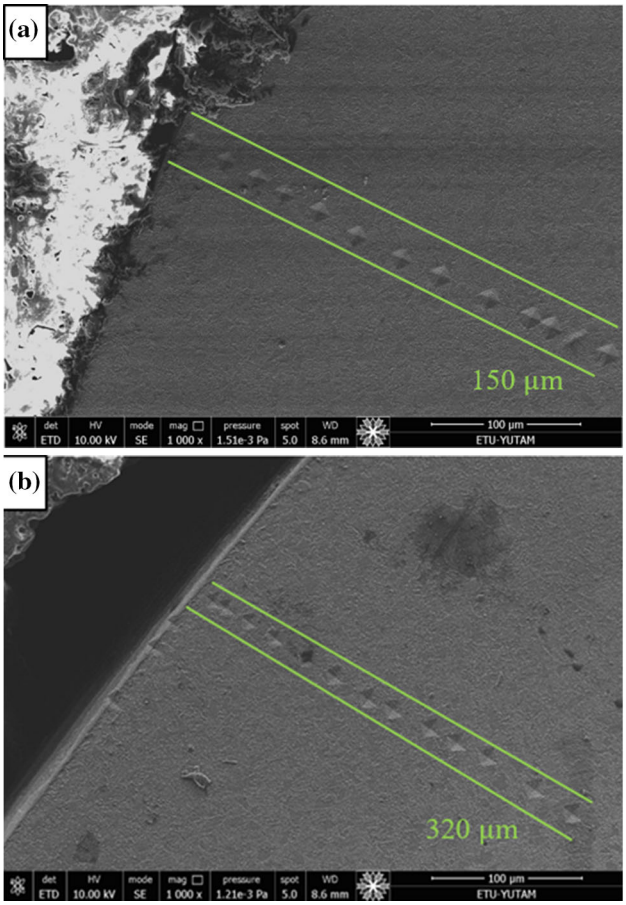

Fig. 6 The cross-section SEM images of microhardness profiles of plasma nitrided specimens: (a) 480 °C for 2 h-PN1 and (b) 480 °C for 9 h-PN2

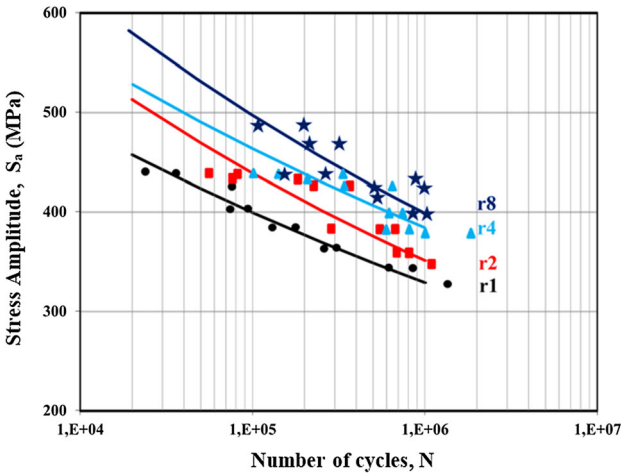

Fig. 7 S-N curves of untreated notch specimens according to the ASTM E739-91(2004)e1 standard Ref 35

K_t = 1.63) samples. The lowest fatigue limit was obtained from the untreated r1 sample and its value was 328 MPa. This is due to the influences of the theoretical K_t. Local stresses are significantly affected by the value of the radii of the notch and therefore, a decrease in the notch radius causes an increase in K_t. While the notch radius is sharp, the fatigue limit is low. However, the fatigue limit is increased because the stress concentrations are reduced i.e., the notch radius is smoothly transitioned.

The S-N curves for PN1 and PN2 conditions are given in Fig. 8. Fatigue limits of both untreated and plasma nitrided notched parts decreased with decreasing notch radius value, with increasing K_t value. The fatigue limit of plasma nitrided notched parts increased compared to untreated notched samples. The fatigue limit of the untreated r1 (K_t = 1.63) sample shown in Fig. 8(a) was increased from 328 to 407 MPa by PN1 condition, while it was increased to 567 MPa by PN2. The fatigue limit of the untreated r2 (K_t = 1.41) sample shown in Fig. 8(b) was increased from 352 to 432 MPa by PN1 condition, while it was increased to 593 MPa by PN2. The fatigue limit of the untreated r4 (K_t = 1.27) sample shown in Fig. 8(c) was increased from 386 to 453 MPa and 650 MPa by PN1 and PN2, respectively. The fatigue limit of the untreated r8 (K_t = 1.19) sample shown in Fig. 8(d) was increased from 401 to 465 MPa and 691 MPa by PN1 and PN2, respectively. The highest fatigue strength (691 MPa) was obtained in the PN2-r8 sample, where the process time and notch radius were the highest. According to these results, the fatigue limits of plasma nitrided notched specimens were higher than the untreated ones. After the plasma nitriding process, the fatigue strength of the samples showed an improvement between 20 and 72%. Up to 72% improvement was achieved in the fatigue limits of the samples with the lowest stress concentration factor and nitrided for long periods.

When the S-N curves of untreated specimens (Fig. 7) are examined, it is seen that fatigue strength of the material is reduced by increasing K_t, as expected. A high K_t value means that the notch is sharp, and stress concentrations around sharp notches are also high. Therefore, fatigue crack starts from the regions where stress concentrations are high due to the effect of cyclic loads, and this has a negative effect on the fatigue life of the material (Ref 41-43). On the other hand, when the S-N curves of the untreated and plasma nitrided samples (Fig. 7 and 8) are examined together, it is seen that the fatigue strength of the material increases for each notch geometry compared to the untreated samples after plasma nitriding. As mentioned earlier, the reason for this is the increase in surface hardness, the formation of compound and diffusion layers and compressive residual stresses on the surface and near the surface of material after plasma nitriding. As it is known, compressive residual stresses have beneficial effects on the fatigue life of materials. In addition, in plasma nitrided samples, the formation of hard surface and subsurface structures makes dislocation movement difficult and hence, the fatigue strength of materials is improved (Ref 16, 44). Therefore, the fatigue strength of the material was improved by these effects through plasma nitriding. However, another significant point is the amount of increment in fatigue strength. When the S-N curves and Table 3 are examined together, it is observed that PN2 specimens exhibit more improvement than PN1 specimens in terms of fatigue strength. While the fatigue strength of the nitrided samples in the PN1 condition increased by around 20%, the increase rate in the nitrided samples in the PN2 condition was around 72%. This shows that the compressive residual stresses and the thickness of the diffusion zone is highly effective on the fatigue strength. As discussed earlier, PN2 had high diffusion zone thickness and compressive residual stresses and therefore, the specimens, which were plasma nitrided at this condition, exhibited higher

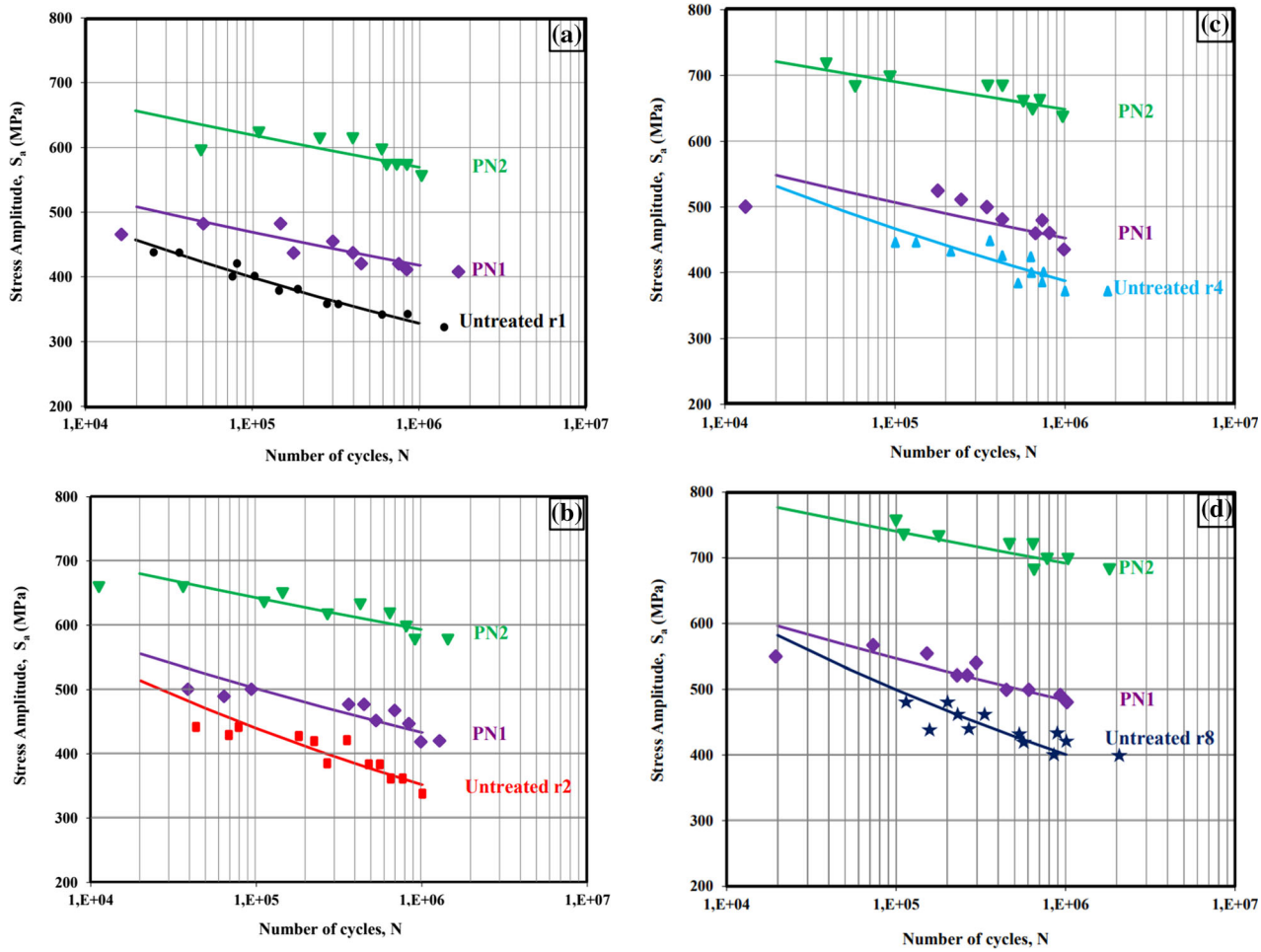

Fig. 8 S-N curves of untreated and plasma nitrided notch specimens according to the ASTM E739-91(2004)e1 standard: (a) r1, (b) r2, (c) r4 and (d) r8 (Ref 35)

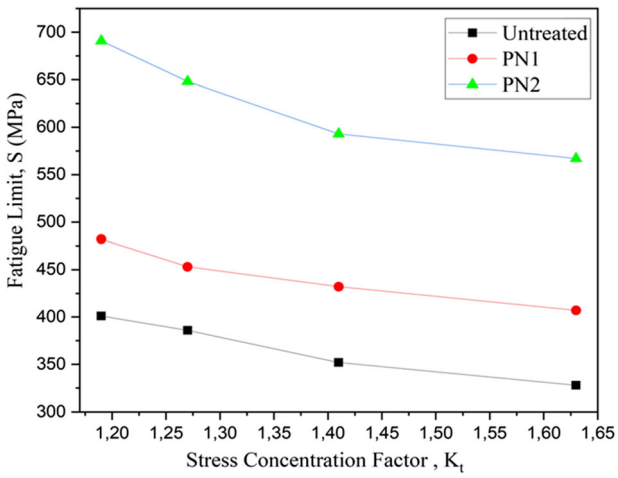

Fig. 9 Relationship between fatigue limit and stress concentration factor

fatigue strength than untreated specimens and plasma nitrided specimens at PN1.

The relationship between stress concentration factor and fatigue limit is shown in Fig. 9. It is understood that there is an approximately linear relationship between fatigue limit and K_t.

Table 5 Constants of linear Eq 1 by curve fitting from Fig. 10

Specimens	A	B	Correlation coefficient, R^2
Untreated	168.21	598.03	0.9669
PN1	172.15	683.46	0.9300
PN2	273.86	1001.30	0.9018

The fatigue limit increased as the K_t decreased with the notch effect. Also, the increase in fatigue strength was found due to increasing nitriding process time. Therefore, an inverse relationship was established between these values as given in Eq 1. Table 5 also shows the constants of Eq 1. It was determined that the correlation coefficients of the linear trend obtained by using the curve fitting method were close to 1. For this reason, it is concluded that the fatigue limit of untreated and plasma nitrided AISI 4140 specimens can be expressed as in Eq 1. Another critical point here is the correlation coefficients. The highest value of the correlation coefficient was obtained from the untreated sample. The K_t and fatigue limit of the untreated sample is more linear than that of the plasma nitrided parts. This can be explained by the structures and mechanical properties of the layers and phases formed after nitriding.

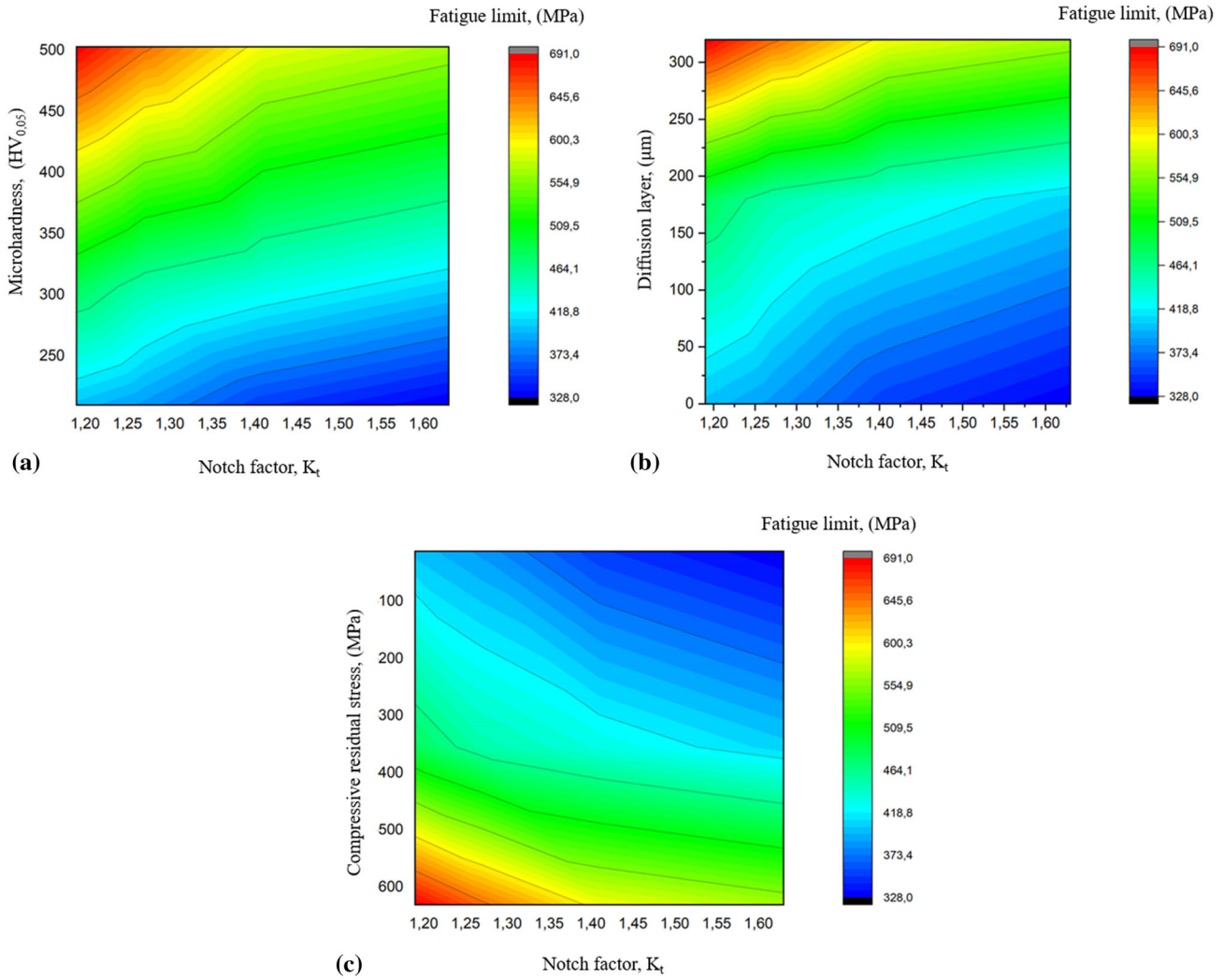

Fig. 10 Design curves presenting the relationship between microhardness, diffusion layer and residual stress on the fatigue limit and notch factor

Although hard and high-strength surface layers are obtained after plasma nitriding, the metallurgical properties of these structures show great variability. For this reason, these changes in nitrided samples cause the relationship between stress concentration factor and fatigue strength to deviate from linearity.

$$S = -A \times K_t + B \quad \text{(Eq 1)}$$

In our experimental study, two different plasma nitriding (PN1 and PN2) process parameters were applied to four different theoretical stress concentration factor values (K_t (1.63, 1.41, 1.27 and 1.19)). The microhardness, diffusion layer depth and compressive residual stress values were determined. These values were correlated with the fatigue limit and the notch factor. The design curves presenting the relationship between the notch factor and microhardness, diffusion layer and residual stresses in terms of fatigue strength are given in Fig. 10. According to these graphs, the fatigue limit of the specimens decreases when the notch factor increases. However, a significant increase takes place in the residual stress, hardness, and diffusion layer thickness of the material with the application of plasma nitriding. Additionally, here, when the desired microhardness, diffusion layer thickness or compressive residual stress values are known for a certain K_t value, the approximate fatigue life of the material can be determined.

Fatigue fracture images of the specimens are given in Fig. 11. The images show that fatigue occurs in three stages: fatigue crack initiation, propagation of the crack in a certain period and the final fracture (Ref 45). The fracture surface of the untreated r1 (K_t = 1.63) sample is shown in Fig. 11(a). This image shows that fatigue crack started on the notch root due to cyclic shear deformation due to the high K_t. The fracture surface of the untreated r2 (K_t = 1.41) sample is shown in Fig. 11(b). Numerous micro cracks were observed on the surface of untreated notched parts. Therefore, it is understood that the crack in the untreated samples starts from the notches where the stress concentrations are the highest. These micro cracks then propagate to the inner section of the sample, and at the last stage, fracture damage occurs. In plasma nitrided samples, fatigue cracks tend to start under the surface due to high surface hardness, the presence of surface and subsurface layers and compressive residual stresses, which cause the prevention of cyclic slip in the surface (Fig. 11(c)). These micro cracks form and propagate under the surface and subsequently cause sudden failure. The fatigue cracking in plasma nitrided

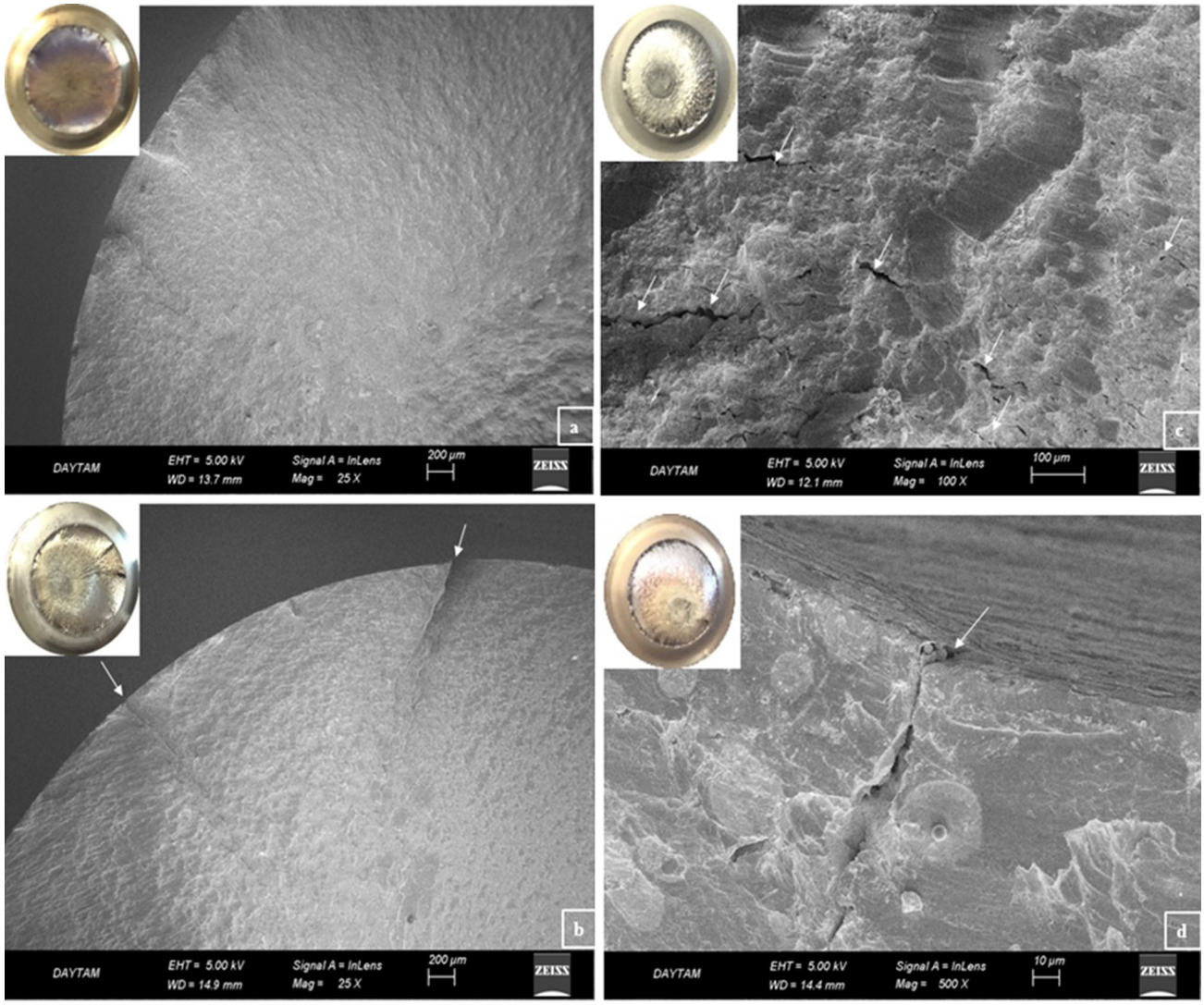

Fig. 11 SEM fractography of notch samples: (a) Untreated-r1 ($S_a = 380$ MPa, $N = 156314$ *cycles*), (b) Untreated-r2 ($S_a = 430$ MPa, $N = 180960$ *cycles*), (c) PN1-r2 $S_a = 480$ MPa, $N = 417243$ *cycles*) and (d) PN2-r1 ($S_a = 600$ MPa, $N = 50321$ *cycles*)

samples generally occurs with this mechanism. Fig. 11(d) shows that the fatigue crack forms at a single point on the surface and this crack causes the fracture. The compound layer containing more than one phase is of high hardness, which causes the compound layer to be more brittle. Therefore, the fatigue crack starts at a single point in the brittle compound layer in this part (Ref 46).

The images showing the fracture surfaces of untreated and plasma nitrided samples are shown in Fig. 12. Transgranular ductile fracture is observed in the core regions of samples. In contrast, Transgranular brittle fracture is seen in the diffusion zone (Fig. 12(a)). The final fracture appearance of untreated and plasma nitrided notched samples is the same. The ductile fracture seen in the core zone of the PN1-r2 sample is shown in Fig. 12(b). The most distinctive feature of ductile fracture is the presence of micro-voids (dimples). The micro-void formation breaks the particles and separates the particle interfaces. Due to the more significant plastic deformation in these disintegrating regions, the section is broken by not being able to carry the applied load anymore. From these observations, it is concluded that transgranular ductile fracture is seen in untreated sample and/or core region of plasma nitrided specimen, whereas transgranular brittle fracture is seen in surface and subsurface layers of plasma nitrided specimens due to the brittleness of these structures (Ref 47, 48).

As a result of the plasma nitriding, in some cases, a structure called "fish-eye" is observed after fatigue fracture. The system of fish-eye crack is as follows: an inclusion under the nitrided layer is subjected to tensile stress and stress concentration occurs at the inclusion-matrix interface. Therefore, the cracks nucleate at the inclusion-matrix interface and form a radially propagating circular crack under tensile stress (Ref 49, 50). While fish-eye formation was not observed in notched parts under PN1 condition, it was observed in notched samples nitrided with PN2 condition. This is because high residual stresses are observed on the surface of notched samples with increasing plasma nitriding time. The typical fish-eye fracture formation was observed in the fatigue fracture surface (Fig. 13).

It has been stated in many different studies in the literature that fatigue cracking does not always start on the surface of the material but it starts in the inner parts of materials due to their hard surface in plasma nitrided materials. In this regard, the results are in accordance with the literature (Ref 19, 20).

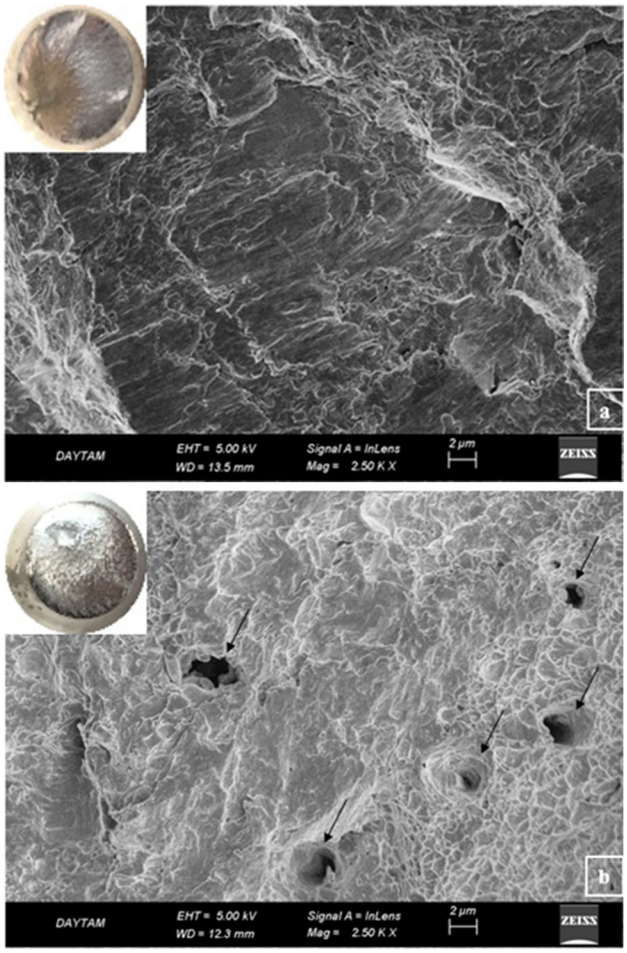

Fig. 12 SEM fractography of notch samples: (a) Untreated-r4 ($S_a = 440$ MPa, $N = 138416$ *cycles*) and (b) PN1-r2 ($S_a = 440$ MPa, $N = 846173$ *cycles*)

4. Conclusions

In the present study, four different groups of specimens with stress concentration factors (K_t) of 1.63, 1.41, 1.27 and 1.19 were produced from AISI 4140 low alloy steel and they were plasma nitrided at 480 °C for 2 h and 9 h. The specimens were subjected to rotating bending fatigue tests and the influences of stress concentration and plasma nitriding on the fatigue strength of the material were investigated. The obtained results of the present study are as follows:

- After plasma nitriding, ε- $Fe_{2-3}N$ and $\gamma\prime-Fe_4N$ phases formed and their intensity were increased by increasing treatment time. Compound layer and diffusion zone were formed on the surface of the samples by plasma nitriding. In addition, diffusion layer thickness increased with increasing plasma nitriding time.
- Compressive residual stresses formed and their amount increased with plasma nitriding time due to the increasing amount of diffused nitrogen atoms. Also, plasma nitriding caused an increase in the surface hardness of the material and its amount increased with plasma nitriding time.
- Fatigue strength of notched specimens were enhanced by plasma nitriding due to increasing hardness and compressive residual stresses formed on compound and diffusion layers. Up to 72% improvement was achieved in the fatigue strength of the notch parts with the lowest K_t and nitrided for long periods.
- Fatigue limit of the material decreased as the K_t increased due the radius size variation. However, plasma nitrided specimens showed higher fatigue limits than untreated specimens and the amount of increase in fatigue limit decreased with increasing K_t value. Also, it was determined that there is an inverse relationship between the stress concentration factor (K_t) and the fatigue limit (S), which can be expressed as $S = -A \times K_t + B$

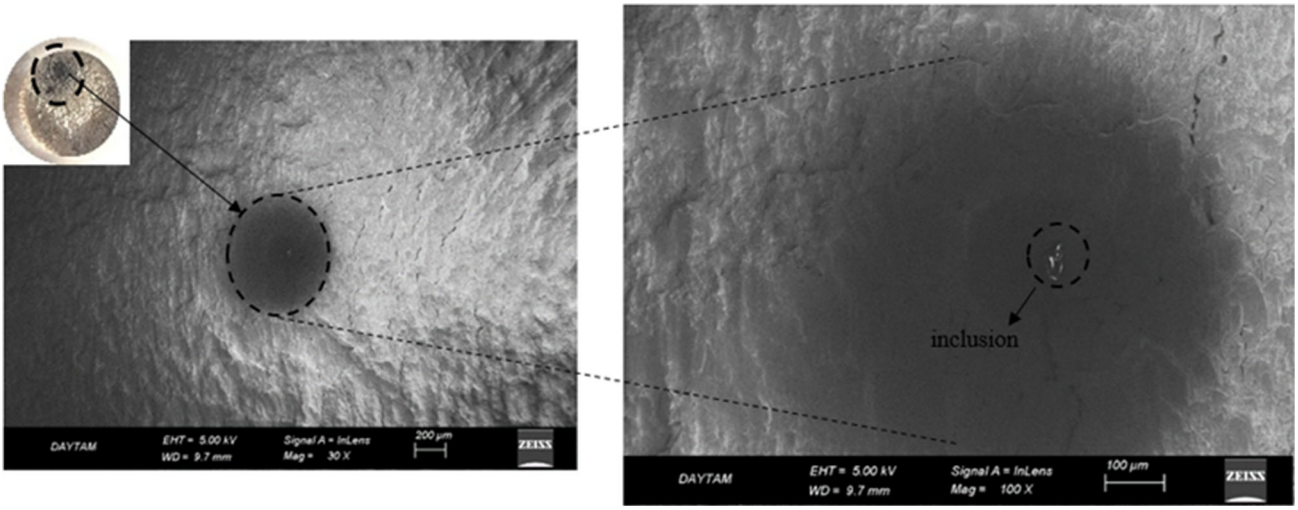

Fig. 13 SEM fractography of fish eye crack formation: PN2-r8 ($S_a = 720$MPa, $N = 464913$*cycles*)

- According to fractographic examinations, it was observed that plasma nitrided specimens (at 480 °C for 9 h) exhibited sub-surface 'fish-eye' type crack formation originating from nonmetallic inclusions. In addition, transgranular ductile fracture was observed in the core of the specimens, while transgranular brittle fracture was obtained in the diffusion layer.

Acknowledgments

The authors would like to thank Atatürk University East Anatolia High Technology Application and Research Center (DAYTAM) and Erzurum Technical University High Technology Application and Research Center (YUTAM) for their assistance.

Author Contributions

F. Yılan: Visualization, Investigation, Validation, Methodology, Writing-original draft, Writing—review & editing. H. Kovacı: Conceptualization, Supervision, Validation, Investigation, Methodology, Writing—original draft, Writing—review & editing.

Conflict of interest

The authors declare that they have no known competing financial interests or personal relationships that could have appeared to influence the work reported in this paper.

References

1. M.A. Rahmat, R.N. Ibrahim, and R.H. Oskouei, Stress Raisers and Its Effect on Fatigue Sensitivity: A Study of Notch and Fretting Fatigue, *Univers. J. Mech. Eng.*, 2013, **1**(3), p 83–91.
2. J.W. Han, S.H. Han, B.C. Shin, and J.H. Kim, Fatigue Crack Initiation and Propagation Life of Welded Joints, *Key Eng. Mater.*, 2005, **297**, p 781.
3. M. Akita and K. Tokaji, Effect of Carburizing on Notch Fatigue Behavior in AISI 316 Austenitic Stainless Steel, *Surf. Coat. Technol.*, 2006, **200**(20–21), p 6073–6078.
4. A. Al-Turaihi, Q.H. Bader, and A. Basim, Notch Effect on Alumiium Alloy Rod under Rotating Bend Fatigue Load, *IOP Conf. Ser. Mater. Sci. Eng.*, 2021, **1094**(1), p 012069.
5. W.Q. Hao, L. Tan, X.G. Yang, D.Q. Shi, M.L. Wang, G.L. Miao, and Y.S. Fan, A Physics-Informed Machine Learning Approach for Notch Fatigue Evaluation of Alloys Used in Aerospace, *Int. J. Fatigue*, 2022, **2023**(170), p 107536. https://doi.org/10.1016/j.ijfatigue.2023.107536
6. S. Bhuiyan, Y. Mutoh, Y. Miyashita, and Y. Ostuka, Notch Effect on Fatigue Strength of Die Cast AM60 Magnesium Alloy, in *Asian Pacific Conference for Materials and Mechanics*, 2009
7. G.H. Majzoobi and N. Daemi, The Effects of Notch Geometry on Fatigue Life Using Notch Sensitivity Factor, *Trans. Indian Inst. Met.*, 2010, **63**(2–3), p 547–552.
8. A.T. Htoo, Y. Miyashita, Y. Otsuka, Y. Mutoh, and S. Sakurai, Notch Fatigue Behavior of Ti-6Al-4V Alloy in Transition Region between Low and High Cycle Fatigue, *Int. J. Fatigue*, 2017, **95**, p 194–203. https://doi.org/10.1016/j.ijfatigue.2016.10.024
9. A.H. Saleh, M.A. Nasser Ali, M.I. Ismail, and A.N. Abood, The Radius Size Variation Effects on Fatigue Strength of AA6061-T6 and AA6061-O Alloys, *IOP Conf. Ser. Mater. Sci. Eng.*, 2019, **518**(3), p 032063.
10. M.A. Terres, N. Laalai, and H. Sidhom, Effect of Nitriding and Shot-Peening on the Fatigue Behavior of 42CrMo4 Steel: Experimental Analysis and Predictive Approach, *Mater. Des.*, 2012, **35**, p 741–748. https://doi.org/10.1016/j.matdes.2011.09.055
11. S.M. Hassani-Gangaraj, A. Moridi, M. Guagliano, A. Ghidini, and M. Boniardi, The Effect of Nitriding, Severe Shot Peening and Their Combination on the Fatigue Behavior and Micro-Structure of a Low-Alloy Steel, *Int. J. Fatigue*, 2014, **62**, p 67–76. https://doi.org/10.1016/j.ijfatigue.2013.04.017
12. H. Weil, L. Barrallier, S. Jégou, N. Caldeira-Meulnotte, and G. Beck, Optimization of Gaseous Nitriding of Carbon Iron-Based Alloy Based on Fatigue Resistance Modeling, *Int. J. Fatigue*, 2018, **110**, p 238–245. https://doi.org/10.1016/j.ijfatigue.2018.01.022
13. C. Zhou, M. Wang, W. Hui, H. Dong, L. Wang, and R. Wu, Rotating Bending Fatigue Properties of Two Case Hardening Steels after Nitriding Treatment, *Mater. Des.*, 2013, **46**(76), p 539–545. https://doi.org/10.1016/j.matdes.2012.08.0615
14. R. Mohammadzadeh, A. Akbari, and M. Drouet, Microstructure and Wear Properties of AISI M2 Tool Steel on RF Plasma Nitriding at Different N2–H2 Gas Compositions, *Surf. Coat. Technol.*, 2014, **258**, p 566–573. https://doi.org/10.1016/j.surfcoat.2014.08.036
15. C. Zheng, Y. Liu, H. Wang, H. Zhu, R. Ji, Z. Liu, and Y. Shen, Research on the Effect of Gas Nitriding Treatment on the Wear Resistance of Ball Seat Used in Multistage Fracturing, *Mater. Des.*, 2015, **70**, p 45–52. https://doi.org/10.1016/j.matdes.2014.12.050
16. H. Kovacı, A.F. Yetim, O. Baran, and A. Çelik, Fatigue Crack Growth Analysis of Plasma Nitrided AISI 4140 Low-Alloy Steel: Part 1-Constant Amplitude Loading, *Mater. Sci. Eng. A*, 2016, **672**, p 257–264.
17. M. Ozturk, F. Husem, I. Karademir, E. Maleki, A. Amanov, and O. Unal, Fatigue Crack Growth Rate of AISI 4140 Low Alloy Steel Treated via Shot Peening and Plasma Nitriding, *Vacuum*, 2022, **2023**(207), p 111552. https://doi.org/10.1016/j.vacuum.2022.111552
18. O. Unal, E. Maleki, and R. Varol, Plasma Nitriding of Gradient Structured AISI 304 at Low Temperature: Shot Peening as a Catalyst Treatment, *Vacuum*, 2019, **164**, p 194–197. https://doi.org/10.1016/j.vacuum.2019.03.027
19. S.Y. Sirin, K. Sirin, and E. Kaluc, Effect of the Ion Nitriding Surface Hardening Process on Fatigue Behavior of AISI 4340 Steel, *Mater Charact*, 2008, **59**(4), p 351–358.
20. S.M.Y. Soleimani, A.R. Mashreghi, S.S. Ghasemi, and M. Moshrefifar, The Effect of Plasma Nitriding on the Fatigue Behavior of DIN 1.2210 Cold Work Tool Steel, *Mater. Des.*, 2012, **35**, p 87–92. https://doi.org/10.1016/j.matdes.2011.09.067
21. M.S. Aghareb Parast, M. Jamalkhani Khameneh, M. Azadi, M. Azadi, M.H. Mahdipanah, and S. Roostaie, Effect of Plasma Nitriding on High-Cycle Fatigue Properties and Fracture Behaviors of GJS700 Nodular Cast Iron under Cyclic Bending Loading, *Fatigue Fract. Eng. Mater. Struct.*, 2021, **44**(8), p 2070–2086.
22. O. Unal, E. Maleki, and R. Varol, Comprehensive Analysis of Pulsed Plasma Nitriding Preconditions on the Fatigue Behavior of AISI 304 Austenitic Stainless Steel, *Int. J. Miner. Metall. Mater.*, 2021, **28**(4), p 657–664.
23. Y. Peng, S. Zhang, Z. Liu, and J. Gong, Notch Fatigue Behavior of Low-Temperature Gaseous Carburised 316L Austenitic Stainless Steel, *Mater. Sci. Technol.*, 2020, **36**(10), p 1076–1082. https://doi.org/10.1080/02670836.2020.1753155
24. P. De La Cruz and T. Ericsson, Influence of Sea Water on the Fatigue Strength and Notch Sensitivity of a Plasma Nitrided B-Mn Steel, *Mater. Sci. Eng. A*, 1998, **247**(1–2), p 204–213.
25. C.M. Suh, J.K. Hwang, K.S. Son, and H.K. Jang, Fatigue Characteristics of Nitrided SACM 645 According to the Nitriding Condition and Notch, *Mater. Sci. Eng. A*, 2005, **392**(1–2), p 31–37.
26. S. Qin, L. Wang, L. Di, C. Zhang, and M. Zhao, Effect of Carburizing Process on Bending Fatigue Performance of Notched Parts of 18CrNiMo7-6 Alloy Steel, *Eng. Fail. Anal.*, 2023, **147**, p 107161. https://doi.org/10.1016/j.engfailanal.2023.107161
27. H.E.R. Lake, Peterson's Stress Concentration Factors Second Edition, by W.D. Pilkey, *Strain*, 1998, **34**(2), p 71.
28. Q. Bader and E.K. Njim, Effect of Stress Ratio and V Notch Shape on Fatigue Life in Steel Beam, *Int. J. Sci. Eng. Res.*, 2014, **5**(6), p 1145–1154.
29. L. Susmel, Notches, Nominal Stresses, Fatigue Strength Reduction Factors and Constant/Variable Amplitude Multiaxial Fatigue Loading, *Int. J. Fatigue*, 2022, **162**, p 106941. https://doi.org/10.1016/j.ijfatigue.2022.106941
30. DIN 50113:1982, Testing of Metallic Materials; Rotating Bending Fatigue Test

31. ASTM E384-11: Standart Test Method for Knoop and Vickers Hardness of Materials
32. Y. Hong and C. Sun, The Nature and the Mechanism of Crack Initiation and Early Growth for Very-High-Cycle Fatigue of Metallic Materials—An Overview, *Theor. Appl. Fract. Mech.*, 2017, **92**, p 331–350. https://doi.org/10.1016/j.tafmec.2017.05.002
33. S.Y. Sirin, Effect of Hot Dip Galvanizing on the Fatigue Behavior of Hot Rolled and Ion Nitrided AISI 4340 Steel, *Int. J. Fatigue*, 2019, **123**, p 1–9. https://doi.org/10.1016/j.ijfatigue.2019.01.001
34. J. Mei, S. Xing, A. Vasu, J. Chung, R. Desai, and P. Dong, The Fatigue Limit Prediction of Notched Components—A Critical Review and Modified Stress Gradient Based Approach, *Int. J. Fatigue*, 2020, **135**, p 105531. https://doi.org/10.1016/j.ijfatigue.2020.105531
35. ASTM E739-91(2004)e1: Standart Practice for Analysis of Linear or Linearized Stress-Life (S-N) and Strain-Life (ε-N) Fatigue Data
36. S.Y. Sirin and E. Kaluc, Structural Surface Characterization of Ion Nitrided AISI 4340 Steel, *Mater. Des.*, 2012, **36**, p 741–747. https://doi.org/10.1016/j.matdes.2011.12.025
37. H. Shen and L. Wang, Influence of Temperature and Duration on the Nitriding Behavior of 40Cr Low Alloy Steel in Mixture of NH3 and N2, *Surf. Coat. Technol.*, 2019, **378**, p 124953. https://doi.org/10.1016/j.surfcoat.2019.124953
38. H.J. Park, B.S. Kim, C.S. Ahn, K.T. Cho, K. Il Moon, and S.S. Kim, Fracture Behavior of Ion-Nitrided AISI 4140 Steel in Accordance with Variable Applied Current Density, *Adv. Mater. Sci. Eng.*, 2022, **2022**, p 1.
39. F.F. Ling, *Residual Stress Measurement and the Slitting Method*, Springer, Berlin, 2007
40. M. Ebrahimi, M.H. Sohi, A.H. Raouf, and F. Mahboubi, Effect of Plasma Nitriding Temperature on the Corrosion Behavior of AISI 4140 Steel before and after Oxidation, *Surf. Coat. Technol.*, 2010, **205**(SUPPL. 1), p S261–S266. https://doi.org/10.1016/j.surfcoat.2010.07.115
41. U. Zerbst, M. Vormwald, R. Pippan, H.P. Gänser, C. Sarrazin-Baudoux, and M. Madia, About the Fatigue Crack Propagation Threshold of Metals as a Design Criterion—A Review, *Eng. Fract. Mech.*, 2016, **153**, p 190–243. https://doi.org/10.1016/j.engfracmech.2015.12.002
42. C. Zhao, W. Zha, J. Zhang, and X. Nie, Surface Fatigue Cracking of Plasma Nitrided Cast Iron D6510 under Cyclic Inclined Contact Stresses, *Int. J. Fatigue*, 2019, **124**, p 10–14. https://doi.org/10.1016/j.ijfatigue.2019.02.046
43. R. Branco, J.D. Costa, F. Berto, A. Kotousov, and F.V. Antunes, Fatigue Crack Initiation Behavior of Notched 34CrNiMo6 Steel Bars under Proportional Bending-Torsion Loading, *Int. J. Fatigue*, 2020, **130**, p 105268. https://doi.org/10.1016/j.ijfatigue.2019.105268
44. G. Ongtrakulkij, J. Kajornchaiyakul, K. Kondoh, and A. Khantachawana, Investigation of Microstructure, Residual Stress, and Hardness of Ti-6Al-4V after Plasma Nitriding Process with Different Times and Temperatures, *Coatings*, 2022, **12**(12), p 1932.
45. U. Zerbst, M. Madia, M. Vormwald, and H.T. Beier, Fatigue Strength and Fracture Mechanics—A General Perspective, *Eng. Fract. Mech.*, 2018, **198**, p 2–23. https://doi.org/10.1016/j.engfracmech.2017.04.030
46. A.F. Yetim, H. Kovacı, Y. Uzun, H. Tekdir, and A. Çelik, A Comprehensive Study on the Fatigue Properties of Duplex Surface Treated Ti6Al4V by Plasma Nitriding and DLC Coating, *Surf. Coat. Technol.*, 2022, **458**, p 129367. https://doi.org/10.1016/j.surfcoat.2023.129367
47. M.S. Mahdipoor, D. Kevorkov, P. Jedrzejowski, and M. Medraj, Water Droplet Erosion Behavior of Gas Nitrided Ti6Al4V, *Surf. Coat. Technol.*, 2016, **292**, p 78–89. https://doi.org/10.1016/j.surfcoat.2016.03.032
48. W. Kong, V.M. Villapun, Y. Lu, L.N. Carter, M. Kuang, S. Cox, and M.M. Attallah, The Influence of Thermal Oxidation on the Microstructure, Fatigue Properties, Tribological and in Vitro Behavior of Laser Powder Bed Fusion Manufactured Ti-34 Nb-13Ta-5Zr-0.2O Alloy, *J. Alloys Compd.*, 2022, **929**, p 167264.
49. P. De La Cruz, M. Odén, and T. Ericsson, Influence of Plasma Nitriding on Fatigue Strength and Fracture of a B-Mn Steel, *Mater. Sci. Eng. A*, 1998, **242**(1–2), p 181–194.
50. L.B. Winck, J.L.A. Ferreira, J.A. Araujo, M.D. Manfrinato, and C.R.M. Da Silva, Surface Nitriding Influence on the Fatigue Life Behavior of ASTM A743 Steel Type CA6NM, *Surf. Coat. Technol.*, 2013, **232**, p 844–850. https://doi.org/10.1016/j.surfcoat.2013.06.110